Performance of a Low-Power Cylindrical Hall Thruster

IEPC-2005-011

Kurt A. Polzin,[*] Thomas E. Markusic,[†] Boris J. Stanojev[‡] and Amado Dehoyos[§]

Propulsion Research Center

NASA - Marshall Space Flight Center

Huntsville, Alabama 35812

Yevgeny Raitses,[¶] Artem Smirnov[‖] and Nathaniel J. Fisch[**]

Princeton University Plasma Physics Laboratory (PPPL)

P.O. Box 451

Princeton, New Jersey 08543

The performance of a low-power cylindrical Hall thruster, which lends itself more readily to miniaturization and low-power operation than conventional (annular) Hall thrusters, was measured using a newly developed thrust stand capable of measuring thrust levels ranging from 1-1000 mN. This test provided an opportunity to demonstrate the stand's mN-level thrust measurement capability. Several new techniques are built into the thrust stand for the purpose of reducing drift in the thrust stand pendulum arm 'zero'-position. An auto-leveling system with feedback control maintains the position of the stand while the temperature is controlled using a constant temperature output water chiller. In addition, the effects of wire heating and deformation are minimized by conducting current onto the pendulum arm through pools of liquid gallium. These accuracy-enhancing measures enabled measurements of cylindrical Hall thruster performance over a power range of 90-185 W. The measured thrust ranged from 3-6 mN, with anode efficiencies and specific impulses spanning 20-27% and 1100-1650 s, respectively. While showing quantitative agreement with literature data obtained using the same thruster, these measurements possessed a smaller uncertainty due to the stability of the thrust stand arm 'zero'-position.

Nomenclature

μ_e	Magnetic Moment, J/T
$I_{\rm sp}$	Specific Impulse, sec
$\mathbf{B}, B$	Magnetic Induction, T
$\mathbf{E}$	Electric Field, V/m
$\mathbf{v_e}$	Electron Drift Velocity, m/s

I.   Introduction

THERE is presently a renewed interest in low power propulsion devices for deep space missions. Specifically, NASA is interested in Hall thrusters that can operate at a relatively constant thrust efficiency (45-55%)

---

[*]Propulsion Research Scientist, kurt.a.polzin@nasa.gov.

[†]Propulsion Research Scientist, markusic@nasa.gov.

[‡]Research Engineer, Madison Research Corp.

[§]Summer Research Student. Presently: Graduate Research Assistant, Purdue University, West Lafayette, IN.

[¶]Physicist.

[‖]Graduate Research Assistant.

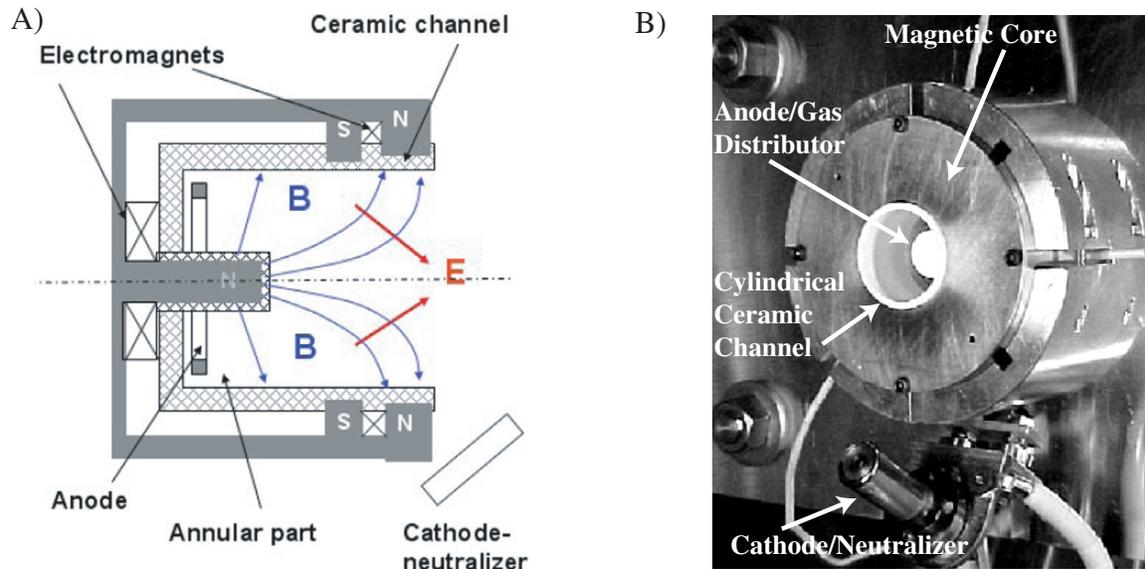[**]Professor, Astrophysical Sciences Dept.

Figure 1. A) Schematic illustration and B) photograph of the PPPL cylindrical Hall thruster.

over a broad power range (300W - 3kW). Recent mission studies[1–4] have shown that a Hall thruster which possesses these performance characteristics is enabling for deep space science missions when compared to ion thrusters.

While Hall thrusters can operate at high efficiency at kW power levels, it is difficult to construct one that operates over a broad envelope down to 100W while maintaining that level of efficiency. Scaling to low power requires a decrease in the thruster channel size and an increase in the magnetic field strength while holding the main dimensionless parameters constant.[5] Increasing the magnetic field becomes technically challenging since the field can saturate the miniaturized inner components of the magnetic circuit and scaling down the magnetic circuit leaves very little room for magnetic pole pieces and heat shields. This makes it difficult to arrive at an optimal magnetic field configuration. Non-optimal fields lead to enhanced power and ion losses which lowers efficiency and results in increased heating and erosion of thruster components, particularly the critical inner components comprising the coaxial channel and magnetic circuit. Erosion of the thruster channel is one of the main life-limiting factors in conventional (annular) Hall thrusters.[5]

An alternative approach presently under study is the cylindrical Hall thruster (CHT) geometry[6–10] illustrated in Fig. 1A. Electrons follow closed azimuthal paths, and the magnetic field lines form equipotential surfaces where $\mathbf{E} = -\mathbf{v_e} \times \mathbf{B}$. Plasma probe measurements have shown that most of the potential drop occurs in the cylindrical region of the channel.[9] The magnetic field topology in the cylindrical geometry may allow for ion acceleration in both the longitudinal direction and towards the thruster axis, potentially reducing ion bombardment and channel wear.

In contrast to the conventional annular geometry, the axial potential distribution is critical for electron confinement in the cylindrical geometry. This is because there is a large axial gradient to the magnetic field over the cylindrical part of the channel. This gradient induces an axial electron drift through the $\mu_e \nabla B$ force, which is in addition to the typical azimuthal electron drift found in conventional Hall thrusters. In the absence of an axial potential, this drift causes the electrons to 'mirror out' of the region of high magnetic field. However, in the cylindrical geometry the axial electric field that accelerates the ions plays an important role in confining the electrons within the thruster by counteracting the axial drift.

Laboratory model CHTs have operated at power levels ranging from the order of 100 Watts up to 1 kW. These thrusters exhibit performance characteristics which are comparable to conventional, annular Hall thrusters of similar size. Compared to the annular Hall thruster, the CHT has a lower insulator surface area to discharge chamber volume ratio. Consequently, there is the potential for reduced wall losses in the channel of a CHT, and any reduction in wall losses should translate into lower channel heating rates and reduced erosion. This makes the CHT geometry promising for low-power applications.

In the present study, the performance (anode efficiency, thrust, I_{sp}) of a 3 cm cylindrical Hall thruster is quantified using the Variable Amplification Hanging Pendulum with Extended Range (VAHPER) thrust stand.[11] Like many other thrust stands, VAHPER measures the relative displacement of a pendulum arm during thruster operation. Thrust stands of this type are typically susceptible to 'zero-drift', which means that when the thruster is turned off, the pendulum arm does not return to its initial position. This phenomenon introduces uncertainty into the relative displacement measurement which, in turn, increases the error on the measured thrust. VAHPER was designed to achieve greater measurement accuracy than other existing thrust stands by minimizing the level of 'zero-drift'.

The outline for the rest of this paper is as follows. In Sect. II we describe the cylindrical Hall thruster tested in this study. The experimental diagnostics and test facility are also described in this section with a focus on the techniques used to reduce 'zero-drift', which enable high resolution thrust measurements. Thrust stand calibration and thruster performance data obtained using the VAHPER thrust stand are presented in Sect. III and compared to literature data obtained using the same thruster. We summarize the main conclusions of this work in Sect. IV.

II.   Apparatus

A.   Cylindrical Hall Thruster

The PPPL 3 cm cylindrical Hall thruster was used for these experiments. The CHT is illustrated schematically in Fig. 1A, while a photograph is shown in Fig. 1B. The thruster consists of a Boron-Nitride ceramic channel, an annular anode, two electromagnet coils, and a magnetic core. The thruster channel is a composite of a shorter, annular region and a longer, cylindrical region. Gas is injected through the anode into the short, annular region of the thruster. The length of the annular region is selected to be approximately equal to the ionization mean free path for xenon. This allows for high ionization of the propellant at the boundary between the annular and cylindrical regions. The electromagnet coils are operated using independently controlled power supplies, and the resulting field topology has a mirror-type structure near the thruster axis.

The working propellant for these experiments was research grade xenon gas. The cathode and anode flowrates were independently controlled using two MKS 0-10 sccm flow controllers (calibrated on Xe). A commercial HeatWave plasma source was used as the cathode neutralizer. In all our experiments, the cathode flowrate was 1 sccm.

B.   VAHPER Thrust Stand

A schematic illustration of the VAHPER thrust stand[11] is shown in Fig. 2. The balance mechanism, located at the top of the figure, uses a series of mechanical linkages to convert horizontal deflections of the hanging pendulum into amplified vertical deflections which are measured using a displacement transducer. Care has been taken to minimize the highly nonlinear effects of friction on the response of the balance. Displacement is measured using a non-contact, light-based linear gap displacement trans-
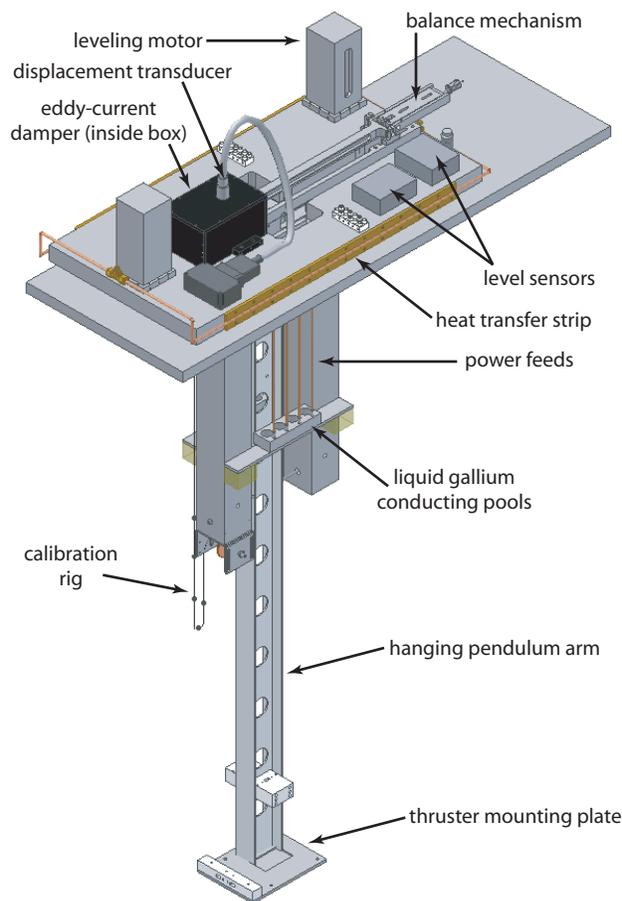
Figure 2. Schematic illustration of the VAHPER thrust stand components.

ducer (LGDT). VAHPER employs flexural pivots which possess no moving parts. Mechanical oscillations induced by thrust fluctuations or external structural vibrations are counteracted using a passive, eddy-current damper, which provides frictionless dissipation of mechanical energy.

Zero drift of the displacement sensor signal is a ubiquitous problem in thrust measurement systems, deriving primarily from unsteady thermal loads and vacuum tank distortions over the course of a test. Consequently, we have incorporated several active control systems into the VAHPER thrust stand design to counteract these effects. These include a level control system and thermal control system. In addition, a new method of conducting current to the thruster was employed in this test to provide additional reduction in the level of drift in the displacement measurement.

The level control system can both sense and counteract deflections of the structure that supports the balance mechanism. Two-axis displacement sensing is performed using a pair of Jewell LSO inclinometers each having a resolution of 0.001^o and a full range of $\pm 3^o$. Two stepper motors are located on the thrust stand, along with one fixed pivot point providing three-point support of the stand. Adjustments in the level of the stand can be made by actuating either (or both) of the stepper motors. Inclinometer data acquisition is performed using a National Instruments PXI system which is interfaced with a NI MID-7604 stepper motor power drive for motor actuation. The motors can be actuated manually or an auto-leveling LabView algorithm can be employed to automatically adjust the motor heights until the inclinometer readings match user-input setpoints.

As the thruster operates, the temperature of the environment inside the chamber climbs. This can cause the support structure to thermally expand over the course of a test, which could greatly alter the displacement signal zero level. To help counteract this, the balance mechanism is mounted on a high thermal inertia, 1.5"-thick aluminum plate. In addition, this plate is actively cooled by water pumped through a closed loop by a programmable output water chiller. In our experiments, the water temperature output by the chiller was held constant at 23° C.

In many thrust measurements, the wires leading to the thruster can greatly affect the level of zero drift experienced over the course of a test (such as in Ref. [12]). The wires experience Joule heating and deformation during thruster operation (especially at high current levels like those used to pre-heat the emitter cathode), which can apply time-varying forces and torques to the thrust stand arm. In the VAHPER thrust stand, this source of drift was eliminated by conducting current onto the thrust stand arm through pools of liquid gallium. Since the wires on the arm were only in contact with the liquid metal, they could no longer apply time-varying loads to the thrust stand arm.

C. Vacuum Facility

The thrust stand is mounted inside a 9-ft diameter, 25-ft long stainless steel vacuum chamber. The vacuum level inside the chamber is maintained by two 2400 l/s turbopumps and two 9500 l/s cryopumps. The base pressure was 5.7×10^{-7} Torr and the background pressure of xenon during thruster operation at ~ 5 sccm total flow rate was $\sim 9 \times 10^{-6}$.

III. Experimental Results and Discussion

A. Thrust Stand Calibration

Displacement (thrust) calibration of the VAHPER thrust stand is accomplished using an in-situ calibration rig to apply a series of known loads normal to the pendulum arm. Calibration can be performed before, during and after thruster operation. The LGDT-measured displacement of the vertically-deflecting linkage is measured and recorded as these loads are applied to the arm. Five known masses are attached at regular intervals on a Kevlar string (see Fig. 2) which is then wound around a spool turned by a stepper motor. The weights can be raised or lowered at any time by remotely actuating the stepper motor. A displacement waveform obtained during a calibration is shown in Fig. 3A. Note the stability in the displacement zero as the stand returns to its initial position roughly 14 minutes after we initiate the calibration procedure.

Calibration measurements and the resulting fit to the data set are plotted in Fig. 3B. An automated data reduction routine is used to analyze the displacement data and generate the curve fit coefficients which can be used to compute thrust. This analysis is performed under the assumption that the relationship between the applied force and the measured displacement is linear. The routine uses an advanced error propagation routine to perform a linear curve fit of the data which takes into account the error bars on the individual
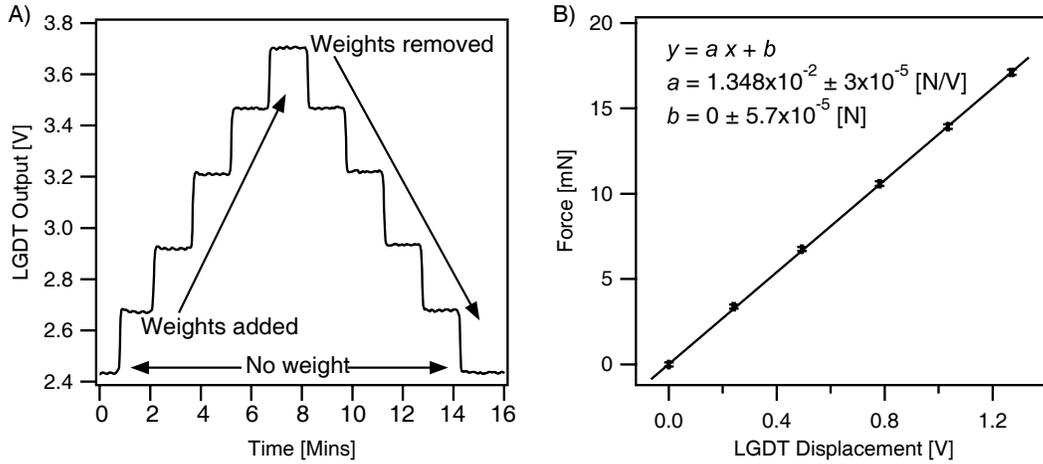
Figure 3. VAHPER thrust stand calibration data. A) Time history showing LGDT measured output as the calibration weights were added and removed. B) Applied calibration force plotted as a function of LGDT displacement. The linear curve is a fit to the data displayed on the graph. Error bars on the datapoints and the fit coefficients represent a 68% (1σ) confidence interval.

force and displacement measurements.[13] Based on the curve fit, we see that the ultimate resolution without the thruster running is $\sim$50 μN.

B. Raw Thrust Data

The output of the LGDT, power supplies and mass flow controllers are recorded throughout the duration of the test. Raw data output by the LGDT is displayed in Fig. 4 for two separate CHT discharge voltages. We immediately see from this figure that there is very little zero-drift in the thrust balance position over this time period. Typically, the largest zero-drifts in past experiments have occurred between the time when the cathode heater is turned on and the discharge is ignited. This is due to the large current level needed to heat the cathode to thermionically emitting temperatures (23 A for our HeatWave cathode). We see in the VAHPER thrust stand data that there is no significant drift associated with cathode heater operation.
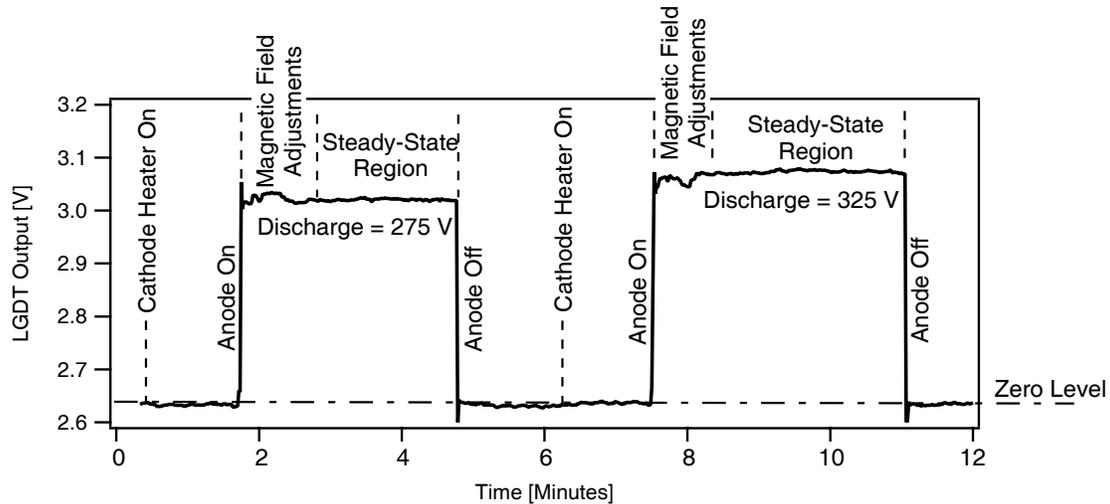

Figure 4. Raw LGDT output data as a function of elapsed time for two thruster operating points.

The thruster operation begins when the emitter cathode becomes hot enough to sustain a thermionic discharge. At this point, the discharge voltage is applied between the cathode and the anode. After the main discharge is activated, the magnetic field coils are energized and adjusted to the desired current levels. As

expected, we observe fluctuations in the raw data trace as the field is adjusted to the final value. Once the field is set, no further adjustments are made, allowing for a 1.5-2 minute steady-state period. After this time period, the discharge is extinguished and the field coils are deenergized in preparation for the next test. We allow enough time between thruster operating points to re-establish the LGDT output baseline (zero level).

C.   Thruster Performance Measurements

The thrust is found by first finding the LGDT output voltage difference between the steady-state portion of thruster operation and the zero level output immediately following thruster shutdown (see Fig. 4). These data are then converted to thrust using the calibration curve-fit constants found in Sect. IIIA. Anode efficiency and I_{sp} are computed according to their standard definitions using the recorded mass flow rates and power supply outputs. The uncertainty levels on the performance data represent a 95% (2σ) confidence interval.
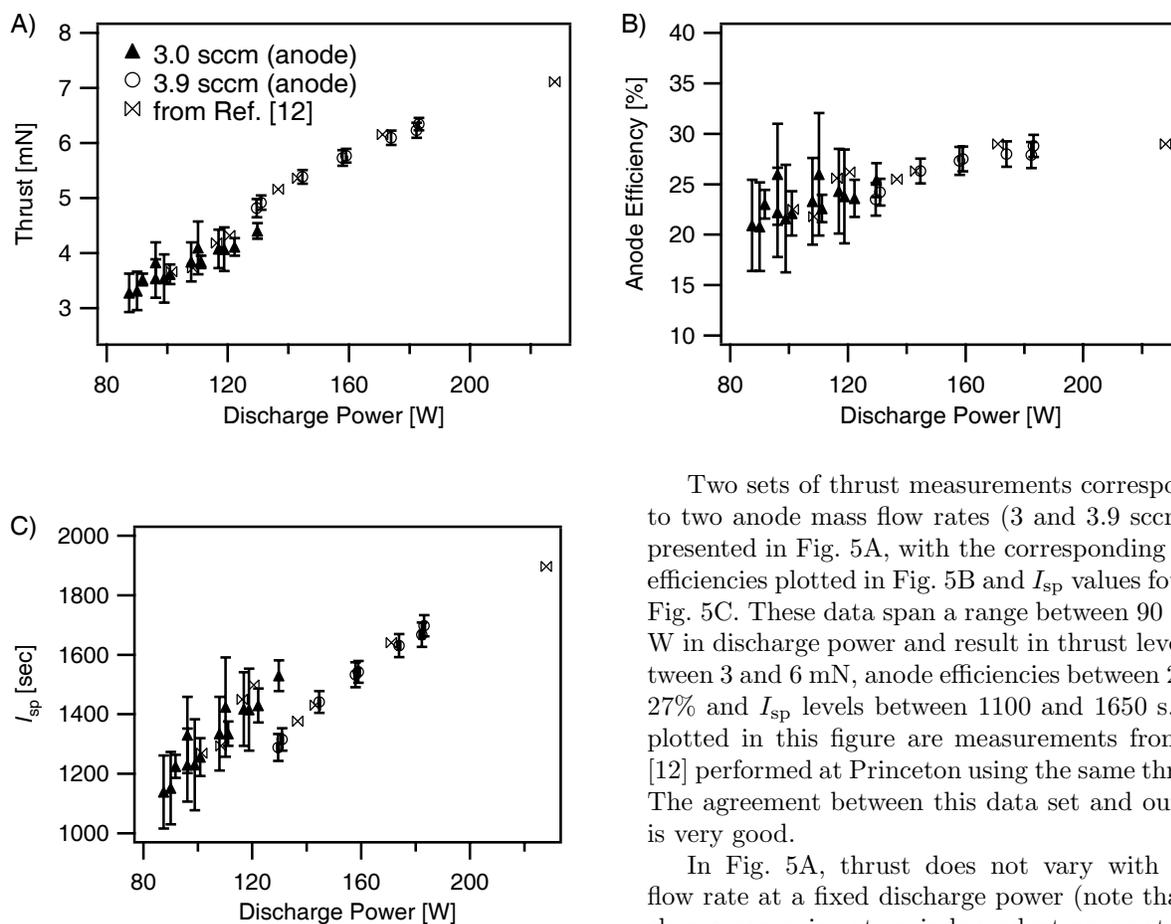
Figure 5. Performance measurements for a 3 cm cylindrical Hall thruster: A) Thrust, B) Anode Efficiency, C) I_{sp} as a function of discharge power. The error bars represent a 95% (2σ) confidence interval. No error bars are displayed on the data from Ref. [12].

Two sets of thrust measurements corresponding to two anode mass flow rates (3 and 3.9 sccm) are presented in Fig. 5A, with the corresponding anode efficiencies plotted in Fig. 5B and I_{sp} values found in Fig. 5C. These data span a range between 90 to 185 W in discharge power and result in thrust levels between 3 and 6 mN, anode efficiencies between 20 and 27% and I_{sp} levels between 1100 and 1650 s. Also plotted in this figure are measurements from Ref. [12] performed at Princeton using the same thruster. The agreement between this data set and our data is very good.

In Fig. 5A, thrust does not vary with anode flow rate at a fixed discharge power (note that discharge power is not an independent parameter in a Hall thruster). Thrust efficiency (Fig. 5B) increases only slightly with discharge power. In addition, it appears to asymptote at the higher power levels. Specific impulse (Fig. 5C) increases with discharge power and also decreases as the anode flowrate is increased, which is not surprising since thrust did not vary with anode flowrate.

In Fig. 5, we observe that the lower power data points possess much larger errors than the higher power points. The larger errors are partially attributable to our not recording enough significant figures in the discharge current measurement for those operating points. The issue was resolved before subsequent testing, but it forced us to estimate the error on the current measurement for these data, which we conservatively overestimated. Additional errors in this lower power set are due to facility-induced drifts in the pendulum

arm position, which were greater during that trial than the second trial in which the higher power data set was acquired. The errors on the higher power (second trial) data set are ∼20% of those associated with the measurements performed at Princeton.[12]

IV. Conclusions

While conventional (annular) Hall thrusters are efficient in the kW power regime, they become inefficient when scaled down to small sizes. This is due to the large insulator surface area to discharge chamber volume ratios and the difficulties associated with maintaining the required magnetic field strength within the thruster at small sizes. The cylindrical Hall thruster can be more readily scaled down to small sizes due to its non-conventional discharge chamber geometry and associated magnetic field profile.

We performed a series of performance measurements on the PPPL 3 cm cylindrical Hall thruster using the VAHPER thrust stand. The thruster produced thrust levels ranging from 3-6 mN, anode efficiencies spanning 20-27%, and I_{sp} between 1100-1650 s. Thrust increased as a function of discharge power while I_{sp} increased with discharge power and decreased with increasing anode flow rate. Comparison of our data set to separate performance measurements acquired at a different facility using the same thruster show good quantitative agreement.

The VAHPER thrust stand provided reproducible data points. Efforts to minimize the zero drift in the baseline resulted in clean, relatively drift-free raw data, leading to high-resolution thrust measurements. Reductions in thermal and mechanical drifts lead to errors on performance measurements that are approximately 20% of those associated with measurements at another facility using the same thruster.

Acknowledgments

References

[1]Oh, D.Y., "Evaluation of solar electric propulsion technologies for Discovery class missions," 41st *AIAA/ASME/SAE/ASEE Joint Propulsion Conference*, July 10-13 2005, AIAA 2005-4270.

[2]Witzberger, K.E., Manzella, D., Oh, D.Y., and Cupples, M., "NASA's 2004 In-Space Propulsion refocus studies for New Frontiers class missions," 41st *AIAA/ASME/SAE/ASEE Joint Propulsion Conference*, July 10-13 2005, AIAA 2005-4271.

[3]Manzella, D., Oh, D.Y., and Aadland, R., "Hall thruster technology for NASA science missions," 41st *AIAA/ASME/SAE/ASEE Joint Propulsion Conference*, July 10-13 2005, AIAA 2005-3675.

[4]Witzberger, K.E. and Manzella, D., "Performance of solar electric powered deep space missions using Hall thruster propulsion," 41st *AIAA/ASME/SAE/ASEE Joint Propulsion Conference*, July 10-13 2005, AIAA 2005-4268.

[5]Morozov, A.I. and Savelyev, V.V., *Review of Plasma Physics*, edited by B.B. Kadomtsev and V.D. Shafranov, Vol. 21, p. 203, Consultants Bureau, New York, 2000, pp. 203.

[6]Raitses, Y. and Fisch, N.J., "Parametric investigations of a nonconventional Hall thruster," *Phys. Plasmas*, Vol. **8**, No. 5, May 2001, pp. 2579; "Cylindrical geometry Hall thruster," US Patent No. 6,448,721, issued Sept. 10, 2002.

[7]Smirnov, A., Raitses, Y., and Fisch, N.J., "Parametric investigations of a miniaturized cylindrical and annular Hall thrusters," *J. Appl. Phys.*, Vol. **92**, No. 10, Nov. 2002, pp. 5673.

[8]Smirnov, A., Raitses, Y., and Fisch, N.J., "Enhanced ionization in the cylindrical Hall thruster," *J. Appl. Phys.*, Vol. **94**, No. 2, July 2003, pp. 852.

[9]Smirnov, A., Raitses, Y., and Fisch, N.J., "Plasma measurements in a 100 W cylindrical Hall thruster," *J. Appl. Phys.*, Vol. **95**, No. 5, Mar. 2004, pp. 2283.

[10]Smirnov, A., Raitses, Y., and Fisch, N.J., "Electron cross-field transport ina low power cylindrical Hall thruster," *Phys. Plasmas*, Vol. **11**, No. 1, Nov. 2004, pp. 4922.

[11]Markusic, T.E., Jones, J.E., and Cox, M.D., "Thrust stand for electric propulsion performance evaluation," 40th *AIAA/ASME/SAE/ASEE Joint Propulsion Conference*, Ft. Lauderdale, FL, 2004, AIAA-2004-3441.

[12]Smirnov, A., Raitses, Y., and Fisch, N.J., "The effect of magnetic field on the performance of low-power cylindrical Hall thrusters," *29th International Electric Propulsion Conference*, Princeton, NJ, Oct. 31 - Nov. 4, 2005.

[13]York, D., Evensen, N.M., Martinez, M.L., and Delgado, J.D.B., "Unified equations for the slope, intercept, and standard errors of the best straight line," *Am. J. Phys.*, Vol. **72**, No. 3, Mar. 2004, pp. 367.